Journal of Atmospheric and Solar-Terrestrial Physics 121 (2014) 123–131

Contents lists available at ScienceDirect

Journal of Atmospheric and Solar-Terrestrial Physics

journal homepage: www.elsevier.com/locate/jastp

Temporal asymmetry in aerosol optical characteristics: A case study at a high-altitude station, Hanle, in Ladakh region

Shantikumar S. Ningombam [a,*], S.P. Bagare [a], A.K. Srivastava [b], V.P. Kanawade [c], Rajendra B. Singh [a,1], Sangita K. Padhy [a,1]

[a] Indian Institute of Astrophysics, 2nd Block Koramangala, Bangalore 560034, India
[b] Indian Institute of Tropical Meteorology, (New Delhi Branch) Prof. Ram Nath Vij Marg, New Rajender Nagar, New Delhi 110060, India
[c] Department of Civil Engineering, Indian Institute of Technology, Kanpur 208016, India

ARTICLE INFO

Article history:
Received 12 June 2014
Received in revised form
30 September 2014
Accepted 1 October 2014
Available online 28 October 2014

Keywords:
Aerosol optical depth
New-particle formation
Desert-dust
Gaseous precursors
Background aerosols

ABSTRACT

Diurnal features of aerosol optical depth (AOD) at a high-altitude station, Hanle (4500 m amsl) in the western Himalayas, were studied using direct/diffuse solar irradiance measurement from a Sky-radiometer (Prede) during October 2007 to December 2010. The study reveals a diurnal asymmetry in the measured aerosol characteristics, with three types of diurnal variation in AOD. Among them, Types I and II are prominent during pre-monsoon, while Type III dominates during post-monsoon. Type I appears to be associated with new-particle formation process from gaseous precursors, in addition to the combination of anthropogenic and desert-dust aerosols, probably brought by the prevailing westerly/south-westerly winds during the pre-monsoon season. The diurnal feature of the Type II may be attributed by the transported desert-dust aerosols brought by the prevailing winds. Further, Type III may be associated with the aged background aerosols over the region, pertaining to a small contribution from gaseous precursors.

1. Introduction

Aerosols exhibit large spatial and temporal variability due to changes in different meteorological factors and/or variability in source and sink processes. Further, diurnal effects of aerosols are largely unknown due to insufficient data coverage globally (Pinker et al., 1994; Kaufman et al., 2000; Smirnov et al., 2002). Due to their short residence time (about a week), aerosols which reside in the troposphere are not uniformly mixed. The sources and sinks of aerosols are widely varied and distributed over the globe such that their physical properties and optical effects show distinct changes with different geographic locations.

Since satellite-based measurements have limited temporal resolution, only the ground-based measurements can provide the diurnal variability of aerosol optical properties. However, diurnal studies of aerosol properties across high-altitude sites, remote, and sparsely inhabited areas of the western and north-western Himalayan regions have been very scarce. Information from such locations assumes a great importance as it provides a sort of aged-background environment against the impact of anthropogenic/dust aerosols transported towards the region (Ram et al., 2010; Srivastava et al., 2012). Such studies can help in understanding the effects of evolving global changes and disturbances on the aged-background condition over a high-altitude clean environment, where the convective, dynamical, and photochemical processes greatly affect the distribution of primary as well as secondary aerosols. Also, it will help in the study of aerosol loading and scavenging phenomena with the dynamical responses of local meteorological conditions. Such studies are also useful to characterize atmospheric new particle formation as reported by Moorthy et al. (2011).

In the recent few years, systematic observations of aerosol optical properties were reported from Hanle (Ningombam et al., 2014a) as well as from a few neighboring regions at Manora Peak (29°24'N, 79°30'E, 1950 m amsl), in the Shiwalik ranges of the Central Himalayas (Sagar et al., 2004) and Mohal (31.9°N, 77.12°E, 1154 m amsl), in the Kullu valley in north-western part of the Himalayas (Kuniyal et al., 2009). Aerosol optical depth (AOD) observed at Hanle is quite comparable with other high altitude remote stations across the globe. An annual mean AOD of 0.05 at 500 nm is reported by Cong et al. (2009) at Nam Co (4720 m amsl), located in the neighboring central Tibetan Plateau. AOD at mountain top of Mauna Loa (3400 m amsl) (Holben and et al., 2001) is 0.02 at 500 nm. Six et al. (2005) have reported AOD value as low as 0.02 for 440 nm at Dome C in Antarctica. Gobbi et al. (2010) have

* Corresponding author. Fax: +91 80 2553 4043.
E-mail address: shanti@iiap.res.in (S.S. Ningombam).
[1] Formerly with Indian Institute of Astrophysics.

http://dx.doi.org/10.1016/j.jastp.2014.10.012
1364-6826/

reported a maximum AOD of 0.08 during May–September and a minimum of 0.04 during winter at 500 nm from the observations taken at the high-altitude (5079 m amsl) station, Himalayan Nepal Climate observatory-Pyramid. However, to our knowledge, no studies of diurnal behavior of aerosol optical properties have been reported so far from the region (western Himalayan region). In the present study, we report the diurnal variation of aerosol optical characteristics from Hanle, in the high-altitude Ladakh region during October 2007–December 2010 using a Skyradiometer observation.

2. Topography of the station and data processing

It may be noted that the entire region of Ladakh is surrounded by high mountain ridges of the Himalayas in the south–east, adjacent to the Tibetan Plateau in the east, and the Karakoram range in the north. The Indus river passes through the Ladakh valley. A Skyradiometer (Model POM-01L, Prede, Japan) was installed at Hanle (32°47'N; 78°58'E, 4500 m amsl) during October 2007 at the hilltop of Mt. Saraswati, adjacent to the 2-m Himalayan Chandra Telescope (HCT) of the Indian Astronomical Observatory (IAO). A high cadence Automatic Weather Station (AWS) was also installed at Hanle during October 2007 at the hilltop, adjacent to the HCT and the panoramic view of the observing station is shown in Fig. 1. The hilltop (~230 m high from the valley) is located in the midst of the Nilamkul plain (4270–4300 m amsl) of Hanle valley in Changthang. The valley is surrounded by mountains with peaks in the range of 5000–5800 m amsl. The valley has a few scattered villages with sparse population of less than 1000, and the main occupation of the villagers is cultivation and cattle rearing. The region has a cold desert climatic condition with annual precipitation/snowfall less than 10 cm (Verma et al., 2010). The station is located very far from industrial/urban-type activities. The nearest town, Leh, is ~260 km away from the site. Monthly average temperature during monsoon (July–August) ranges from 13 °C to 15 °C, while during winter (January–February) it varies from −10 °C to −14 °C. It is extremely dry so that during peak winter, day-time relative humidity (RH) reaches even below 10% on many occasions. The prevailing wind direction is predominantly westerly/south-westerly, for about 70% of the time. The monthly average wind speed in monsoon and winter months is around 4–5 m s^{-1}. The general pattern of wind at the site is such that the speeds are a few m s^{-1} in the early morning hours, picking up to 5–6 m s^{-1} by 10-11 h in the forenoon and reaching peak values in the range of 15–20 m s^{-1} during the afternoon hours to evening. It returns to relatively low values thereafter and remains so throughout the night. Further details of topography and meteorological parameters of the station are described by Ningombam et al. (2014a).

The Skyradiometer measures direct and diffuse solar irradiance at wavelengths 400, 500, 675, 870 and 1020 nm with bandwidths of 10 nm at each of the wavelengths. The measured monochromatic irradiance data were processed to estimate AOD, single scattering albedo (SSA), and aerosol volume size distribution using Skyrad.Pack code (version 4.2, Nakajima et al., 1996). The input of the skyrad.pack software is sky irradiances measured in the almucantar geometry at different scattering angles. As auxiliary data sets such as surface reflectance, atmospheric pressure, and total column ozone are necessary to run the software. The total column ozone was taken from the Ozone Monitoring Instrument (OMI) (Levelt and et al., 2006), and the seasonal and monthly variability of total column ozone were also checked and examined with the results reported by Ningombam (2011). Calibration of the instrument such as solid view angle (SVA) and calibration constant (F0s) at the five filters are performed at regular interval (i.e, every month) and the fresh calibrated values are updated in code. The percentage deviation of SVA during the last three years period is found to be stable with less than 1.0 % (i.e mean deviation) from the initial values estimated by the Prede Engineers at the site during the initial installation. The uncertainties of observed AOD due to such variations in the SVA is negligible (~variation in the 3rd decimal places). Further, the uncertainties of estimated F0s in the present study are within 2% and the resulting uncertainties of

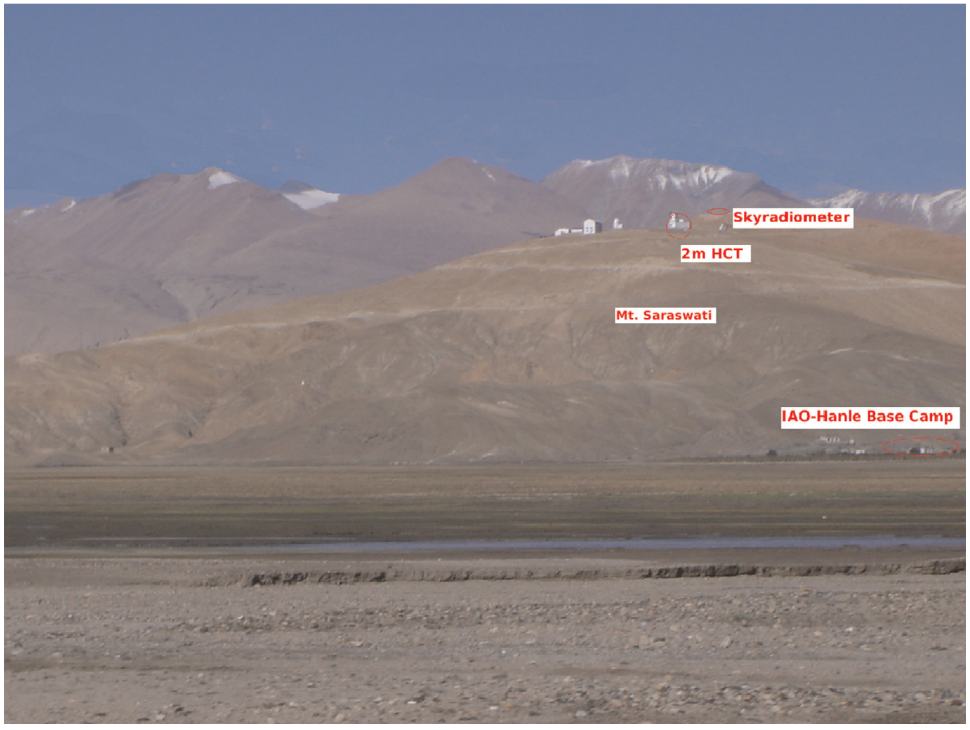

Fig. 1. Panoramic view of the observing station, IAO-Hanle, 2-m HCT, and Skyradiometer at the hilltop of Mt. Saraswati.

AOD and SSA are within 0.02 and 0.03, respectively at 500 nm. The operational details and errors associated with the instrument are described by Ningombam et al. (2014b). The estimated parameters were cloud screened using the code described by Khatri and Takamura (2009).

3. Synoptic conditions over the station

The role of surface wind on evolving aerosols is a complex phenomenon (Smirnov et al., 1995), since under favorable meteorological conditions, strong surface winds may either bring fresh aerosols towards the observational site or may sweep the residing aerosols away (Srivastava et al., 2012b). Our study of monthly mean climatological wind pattern generated from a reanalysis of the data set of the National Centers for Environment Prediction (NCEP) suggests the dominance of winds from west and southwest directions during most of the seasons. Fig. 2 shows the seasonal synoptic wind vectors drawn at 600 hPa. As seen in the figure, a persistent westerly wind flow of airmass arrives toward the observing station in most of the seasons except for monsoon (June–August). However, during the monsoon months, there are two types of air mass arrivals towards the site, one from north–east and another from north-westerly direction. It may be noted that the deserts in the western Asia (including Thar in India and Arabian deserts in the middle East), and Saharan desert in northern Africa are located towards the south–west of the observing station, while Gobi and Taklamakan deserts in Central Asia are located towards north–east and north of the observing station, respectively. The characteristics of desert-dust aerosols are well described by Toledano et al. (2009),Che et al. (2011), McKendry et al. (2007). In addition to the desert-dust, the site is occasionally affected by anthropogenic aerosols, apparently through long-range transport from west/south-west region. In the earlier studies (Ningombam et al., 2014a), presence of anthropogenic and desert-dust aerosols at the altitude of 5–7 km amsl over the present station were noticed from Cloud-Aerosol Lidar and Infrared Pathfinder Satellite Observation (CALIPSO) images (Powell et al., 2009), with air masses arriving from north–west and occasionally from north–east during strong pre-monsoon inflow. As a result, the enrichment of desert-dust and anthropogenic aerosols, including black carbon (BC), leads to relatively higher AOD values during pre-monsoon over this station. In addition to that, Babu et al. (2011) also reported significant contribution of BC over the same station. The study further reported the highest values of BC concentration as 109 ± 78 ng m^{-3} during pre-monsoon and the lowest as 66 ± 42 ng m^{-3} during monsoon.

Diurnal variations of AOD are very significant at low altitudes especially at locations close to densely populated areas, where the evolution of planetary boundary layer (PBL) plays an important role. Neitola et al. (2011) have reported new particle formation (NPF) events at the Himalayan foothill, Mukteshwar (2180 m amsl, close to Nainital). This study reported that frequent occurrence of NPF at such high-altitude, remote, and clean environment with the evolution of the boundary layer is highest (about 2600 m amsl) during pre-monsoon, and moderate (about 1200 m amsl) for rest

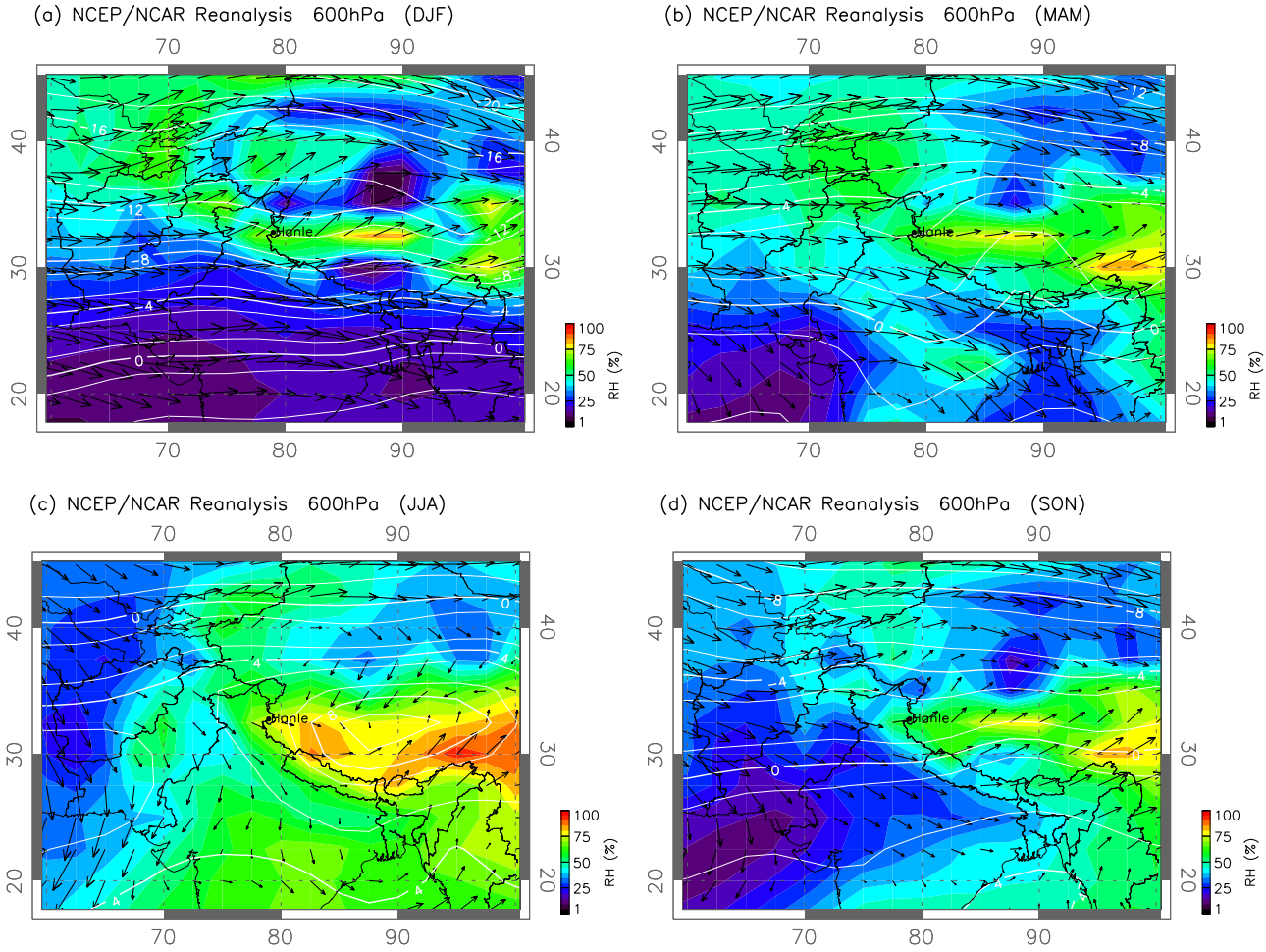

Fig. 2. Seasonal mean (Winter (DJF), pre-monsoon (MAM), monsoon (JJA), post-monsoon (SON)) climatological wind pattern at 600 hPa during 2008–2010 over the Indian region. The *arrows* show the wind direction and the *star* indicated the observing station, Hanle.

of the year. Recently, a significant influence of mineral dust aerosols, transported from the south Asian desert regions and biomass burning aerosols from the north-western parts of India, mostly due to agricultural fires, are reported at Manora Peak in the central Himalayan station during summer (Kumar et al., 2011; Srivastava et al., 2011, 2012b).

4. Results and discussion

4.1. Diurnal variation of AOD

In the present work, the diurnal variation of AOD was examined during four conventional seasons, winter (December–February), pre-monsoon (March–May), monsoon (June–August) and post-monsoon (September–November). The 234 days of cloud screened data with a total of 4777 data points, nearly about 20 points per day on an average, over three years of observations were classified into three distinct types of diurnal variations. In the analysis, days which have only forenoon or afternoon data as well as the days which have less than six data points per day were not included. Such selected days were again checked if there were simultaneous measurement of meteorological parameters and days with missing meteorological observations were excluded from the analysis. By virtue of these data selection criteria, about 58% of the observational data have been rejected. However, this was found to be an essential protocol to maintain the quality control of the data product. In the analysis, mainly three types of diurnal variation in aerosols were noticed such as (a) Type I: the highest AOD of the day in the forenoon, which gradually decreases in the afternoon and further in the evening, (b) Type II: AOD starts gradually increasing from forenoon to afternoon, attaining a maximum towards the end of the day, and (c) Type III: AOD, which is low in the forenoon as well as in the afternoon, increases gradually around local noon-time. Within the Type III, there are a few cases where the AOD variation is very small (less than 10% of the daily mean). This behavior may be attributed to the presence of aged background aerosols. The distribution of the Types I, II, and III is contributed about 66 (28%), 41 (18%), and 127 (54%) days, respectively as shown in Table 1. The diurnal AOD for the three different types is plotted in Fig. 3(a,b,c) at 400, 500, 675, and 870 nm. The vertical bars indicate the standard deviations.

Following the method applied by Smirnov et al. (2002), the percentage deviation of AOD from the daily means was computed for the three different diurnal AOD types. Fig. 4(a,b,c) shows the percentage deviation of AOD at 400, 500, 675, and 870 nm for different types of AOD observed at the site. For Type I, the departure is gradually decreased from peak of 26% in the forenoon at 7:30 h to minimum −28% towards the end of the observation at 16:00 h. The phenomenon is prominently occurred during pre-monsoon and there is a small contribution during post-monsoon, which is characterized by dry and cold surface temperature with

Table 1
Distribution of cloud-screened days for the three AOD types during October 2007–December 2010.

Observed seasons	Types			Cloud-screened total days
	Type I	Type II	Type III	
Winter	9	6	12	27
Pre-monsoon	31	21	18	70
Monsoon	6	7	18	31
Post-monsoon	20	7	79	106
Total	66	41	127	234

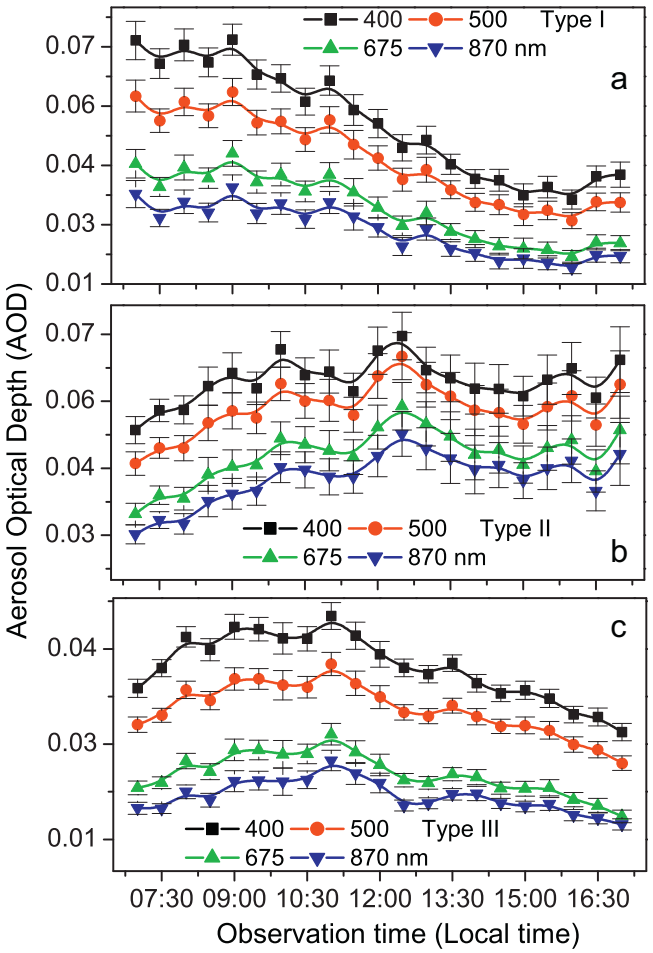

Fig. 3. The different types of averaged diurnal variation of AOD (a,b,c) observed at the site during the entire period of observation. The vertical bars in the graph represent the standard deviation associated in the same type observed during the same time interval.

relatively less windy conditions. For the Type II, the departure starts increasing gradually from minimum −17% at 7:30 h in the forenoon and then it reaches a peak of +20% around at 12:30 h in the afternoon, which prominently occurs during pre-monsoon. The trend further decreases but it remains as +ve departure (+ve 7%) till the end of the observation (17:00 h). The high AOD during afternoon and the low AOD in forenoon have a similar trend of diurnal wind pattern at the site. The ground convective activity during pre-monsoon is high and the process may be enhanced by the stronger wind in the afternoon. Such a process may be attributed to the positive departure of AOD in the afternoon. For the Type III, the trend increases gradually from minimum −10% at 7:00 h till 9:30 h and then it decreases for a while then it reaches a peak of 19% around 11:00 h in the forenoon. Then, the departure decreases to minimum of −26% till evening (17:00 h). The Type III feature is seen in all the seasons but it has a maximum occurrence during post-monsoon.

The estimated mean AOD at 500 nm for the Types I, II, and III is 0.05, 0.06, and 0.04, respectively. In the present work, we defined the aged background level of AOD at 500 nm at the station to be around 0.04, which is close to the yearly mean of 0.044 for the site. We also noted the threshold value of Ångström exponent (α) to be around 0.8 as the line-marked in between the fine and the coarse mode of aerosols as reported by Ningombam et al. (2014a). Further, Kaufman et al. (2000) defined the large dust particles (super-micron radius) as $\alpha < 0.7$ and those due to pollution or the smoke particles (sub-micron radius) as having $\alpha > 1.8$. Between these two

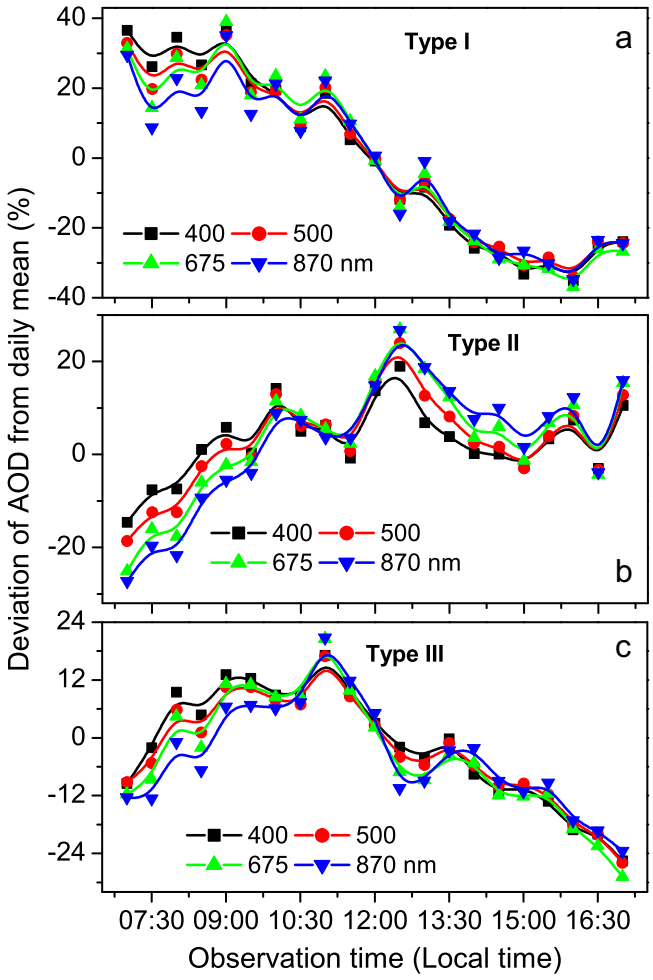

Fig. 4. Percentage deviation of diurnal variation in AOD from its daily mean observed at 500 nm for the different types of AOD (a,b,c) observed at the site.

thresholds are the aerosols in a mixture of the two modes. Table 2 shows the average values over all data points and percentage distribution below critical values for both AOD and α for the three types. It is noticed that the Types I and III have a mixture of the fine and coarse mode of particles defined by the above two thresholds, while Type II is dominated by coarse-mode aerosols.

It is clear from the above results that Type I is found to be most prominent during pre-monsoon with a small contribution during post-monsoon, which is characterized by moderately dry (mean RH 23%) and cold ground temperature (~0 °C) with relatively less windy (~3 m s^{-1}) conditions. Such meteorological conditions are suitable for gas-to-particle conversion processes (i.e. NPF) from gaseous precursors (Neitola et al., 2011 and Moorthy et al., 2011). The NPF frequency shows seasonal cycle with maximum in pre-monsoon and weak in post-monsoon and winter seasons (Neitola et al., 2011). Further, the site is experienced by significant

Table 2
Mean and percentage distribution of AOD at 500 nm, and Angstrom exponent (α) for the three AOD types.

Diurnal	AOD		α	
AOD types	Mean	Below 0.04 (%)	Mean	Below 0.8 (%)
I	0.05	50	1.03	30
II	0.06	30	0.65	70
III	0.04	70	0.93	30

contribution of BC over the station with a maximum in pre-monsoon and minimum in monsoon/winter (Babu et al., 2011). It may be noted that the Himalayas form a barrier for the passage of dust storms resulting in the accumulation of dust particles, largely extended over north-western India and the foothills of the Himalayas. Such dusty events are strongly prominent during pre-monsoon, combined with the heavily evolved atmospheric pollution over northern India, and resulting maximum of aerosol loading during the season (Gautam et al., 2009). Type II, which prominently occurred during pre-monsoon, is characterized by strong convective activity, enhanced by the stronger winds in the afternoon, and can be explained with desert-dust aerosols carried by the prevailing westerly/south-westerly winds. The degree of such convective processes depends on seasons and is strong during pre-monsoon and monsoon seasons. The process became very weak during winter season. During monsoon season, aerosols generated by the strong convective motion has reduced to minimum due to rain-washout (or snowfall) and cloud-scavenging processes. Thereafter, the process has resulted in the formation of diurnal Type III, pertaining to the aged background aerosols in addition to the gas-to-particle conversion (although small contribution) from gaseous precursors.

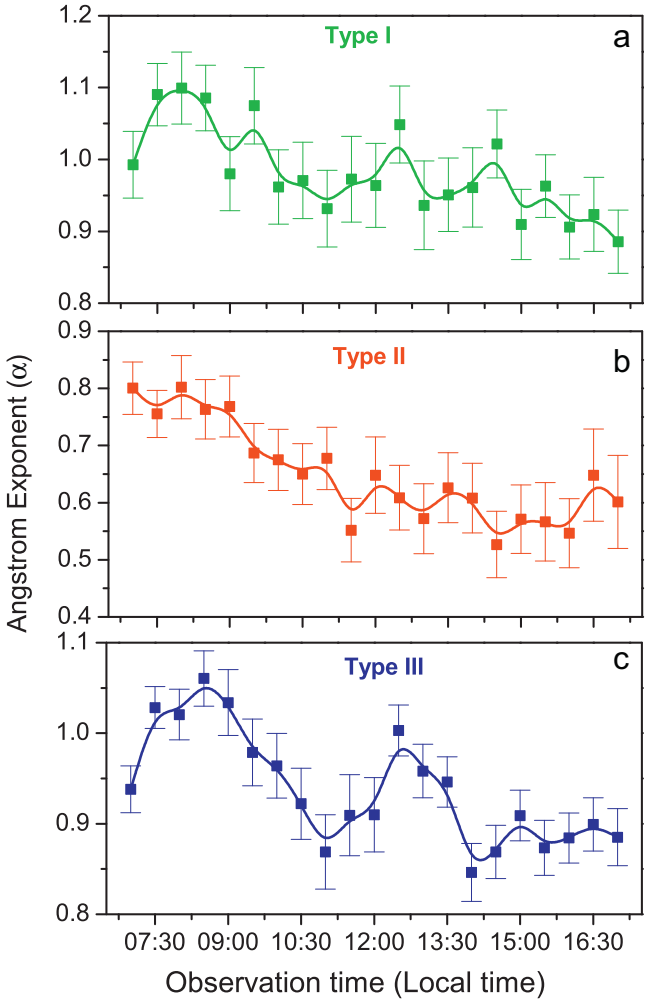

Fig. 5. Average diurnal variability of α for the different types of AOD (a,b,c) observed at the site. The trend reveals the opposite variation of AOD. The smaller α corresponds to coarse-mode particles and high α represents the fine-mode particles.

4.2. Diurnal variation of Ångström exponent (α)

Fig. 5(a,b,c) shows the diurnal variability of α pertaining to the three different types of diurnal cases observed at the site. As reported earlier, due to dry and free tropospheric height and the abundant global irradiance, the site has favorable environmental conditions for the process of new-particle formation from gaseous precursors, probably carried by the strong westerlies/south-westerlies that prevail during pre-monsoon season. This may explain both the increase in AOD and α in the early morning for the case of diurnal Type I. In Fig. 5(a), an increase in α is observed till 07:30 h Local Time from there a gradual decrease is observed till the end of the measurements in a day. Further, as the season advances, the activities are much stronger during pre-monsoon and monsoon seasons due to strong convection processes and this results in relative dominance of coarse-mode particles in the atmosphere (associated with the smaller α value) as in the case of Type II (although small as 18% of the total days) seen in Fig. 5(b). In the figure, the α decreases gradually from morning to evening which may be attributed by the higher wind speed (10–15 m s^{-1}) in the afternoon. The variation in α is found to be by and large similar with the case of Types I and III as seen in Fig. 5(a,c). Such results may be associated with the potential emission sources at the site through photochemical reaction involving from gaseous precursors as reported by Moorthy et al. (2011). Further, as reported therein, morning high events and afternoon low events of particle number concentration (1500–2000 cm^{-3}) during post-monsoon are similarly matched with the present diurnal variation in AOD Type III. The shifting of morning peaks from pre-monsoon to post-monsoon (as in the case of Type I and III) appears to be associated with the shifting of peak solar radiation time as the season advances as reported therein.

The mean α values at the station for Types I, II, and III are found to be 1.03 ± 0.04, 0.65 ± 0.05, and 0.93 ± 0.03, respectively. The moderately high values of AOD of the Type I indicate the small contribution of fine-mode (high α from anthropogenic aerosols) and coarse-mode aerosols (low α from desert-dust) in addition to the sources apparently from gas-to-particle conversion process as discussed above. For example, Type I contributes to the significant features of the anthropogenic aerosols as seen on 30 April (AOD/α:0.08/1.37) and 1 May (0.073/1.34) of 2008; 18 March 2009 (0.10/1.17) and 3 April 2010 (0.08/1.25), as well as the desert-dust aerosols features as seen on 8 April (0.11/0.29), 29 April (0.14/0.46), and 3 May (0.08/0.39) during 2008, and 18 March 2009 (0.07/0.72). These dust and anthropogenic features of aerosols are also noticed from the CALIPSO as reported by Ningombam et al. (2014a). Some of these desert-dust cases reported in Type I are transported from north and north–east of the observing station. It may be noted that about 15% of the wind is coming from north and north–east directions, while westerly/south-westerly winds contributed to about 70%. Type II is dominated by the strong signature of desert-dust aerosols. However, Type III does not show any strong signatures of anthropogenic events as well as desert-dust events, indicating mostly the aged-background aerosols in addition to apparently small emission sources at the site through photochemical reaction from gaseous precursors as discusses above.

4.3. Influence of meteorological parameters on AOD and Ångström exponent (α)

In order to examine the influence of various meteorological parameters on the diurnal variation of AOD, we used surface meteorological parameters (temperature, relative humidity and wind speed) recorded from the AWS at every 5 s interval. However, we extracted the AWS parameters with the same time of skyradiometer observation. Fig. 6(a,b,c) shows the average diurnal variation of meteorological parameters over the site for different diurnal types. The vertical bars in the graph represent the standard errors. The Temperature trend follows a general feature by all the types, which exhibits a minimum at ~7: 30 h in the forenoon and a maximum around ~15: 00 h in the afternoon. Among the trends, Type II resembles the diurnal temperature. The observed daily average temperature of the Types I, II, and III is 0.21, 2.0, and 4.0 °C, respectively. Further, the general trend of diurnal RH is followed by all the types with a maximum around ~7:00 h in the morning and a minimum at ~16: 00 h in the afternoon. The average RH values recorded by Types I, II, and III are 23.0%, 20.0%, and 19.0%, respectively. The maximum and the minimum trends of RH are followed by the Types I and II, respectively as seen in Fig. 6(b), although with a small variation. Fig. 6(c) shows the diurnal trend of surface wind speed for the different types of diurnal AOD. The average wind speed of the Types I, II, and III is 3.0, 5.0 and 4.0 m s^{-1}, respectively. Although there are marginal differences, the Type II exhibits slightly heavier wind speed than Types I and III. The prevailing wind direction for all the cases shows the dominance of south-westerly wind and generally, wind starts gradually rising from the early morning (~0 – 3 m s^{-1}) to a peak value of ~15 – 20 m s^{-1} between the afternoon and late evening, as stated earlier. However, the wind settles down to minimum (~ 0–5 m s^{-1}) during the night. This pattern is uniform at the site irrespective of the seasons.

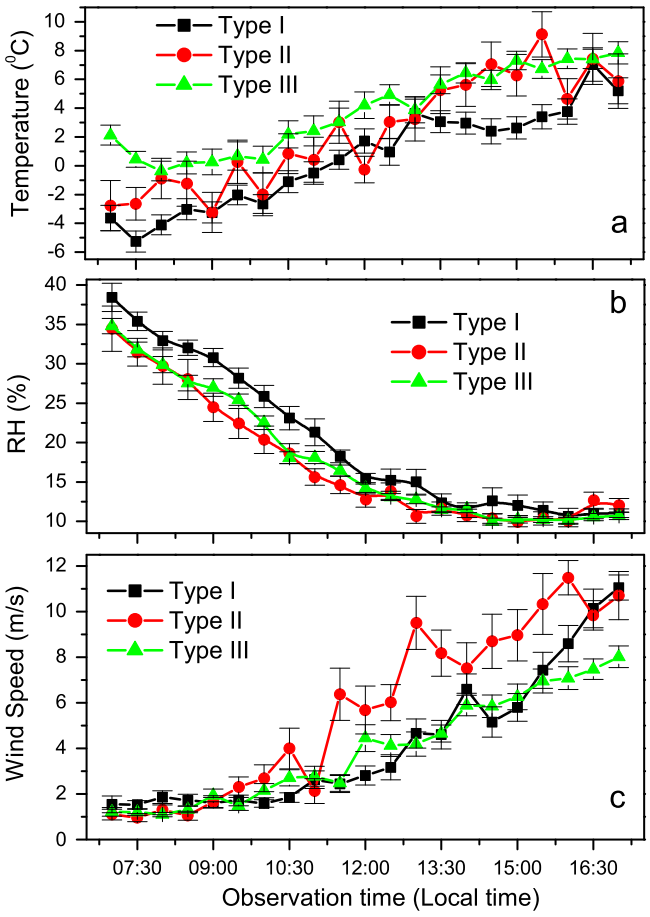

Fig. 6. Average diurnal variation of surface meteorological parameters [(a) temperature, (b) relative humidity, and (c) wind speed] over the site for the different types of diurnal variation in AOD. The vertical bars in the graph represent the standard errors associated while averaging the meteorological parameters on the same group from different days from different months at the same time interval.

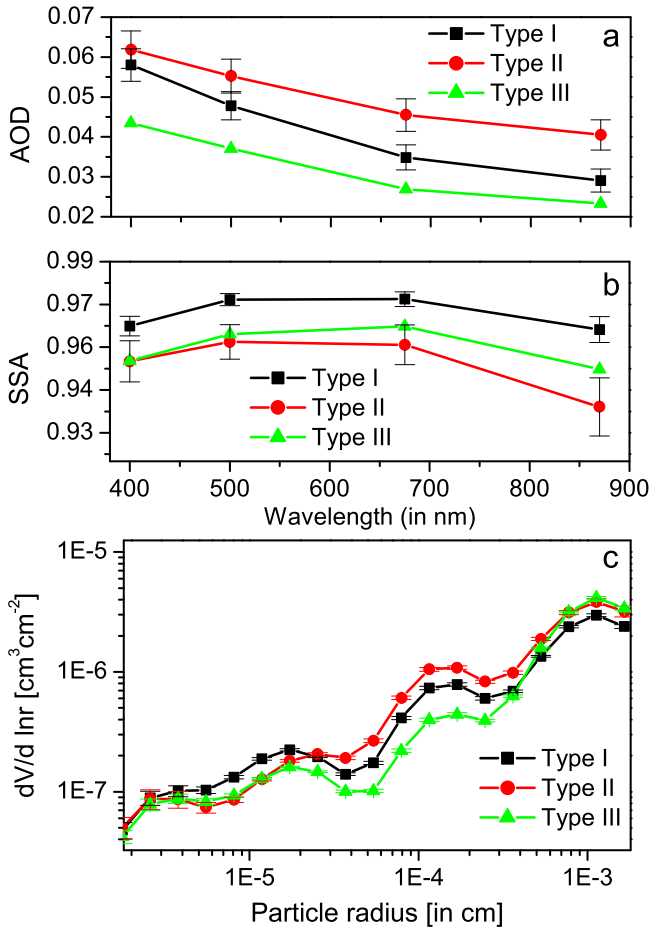

Fig. 7. Spectral variation of averaged (a) AOD, (b) SSA, and (c) aerosol volume size distribution of three different types of diurnal case study.

4.4. Spectral variation of AOD and SSA with the aerosol size distribution

Fig. 7(a) shows the spectral variations of AOD for different types of diurnal case in the present study. As reported by Ningombam et al. (2014a), the station is characterized by the dominance of non-absorbing aerosols with tri-modal volume size distribution, which is indicated by coarse-mode aerosols of desert-origin. Such non-absorbing features (high SSA) are seen in Fig. 7(b) for the Types I and III, while Type II indicates a moderate absorbing feature with the mean values (SSA at 500 nm) as 0.976, 0.969, and 0.962, respectively. For example, daily mean SSA for the desert-dust case on 8 April 2008 has 2.38% higher (0.990) than the anthropogenic case on 30 April 2008 (0.967) but both the days are contributing to the Type I.

Further, as reported by Ningombam et al. (2014a), the influx of aerosols (either anthropogenic or desert-dust) at site is transported mostly from west and south–west (~70%) regions and occasionally from north and north–east (~15%), where Taklamakan and Gobi deserts are located. Liu and et al. (2008) have reported that mineral dust from west Asian deserts (or even from Sahara) can contribute to a large fraction of aerosols, particularly during pre-monsoon, when dust is observed to mix with anthropogenic pollutants. Further, Seinfeld and et al. (2004) have reported that dust transported from east Asia to the Pacific does not absorb as much as aerosols from south Asia or from the Sahara desert. In this context, the high AOD of the Types I and II may be contributed to mix with desert-dust and anthropogenic aerosols, which may have moderate high values of α (fine mode) at the station. Fig. 7(c) shows dominance of tri-modal volume size distribution observed even in the three Types of diurnal cases. Although all the trends appear to be more or less similar, Type II indicates the highest coarse-mode (small difference) aerosols from the rest of the two Types as seen in the Fig. 7(c). Such dominance of tri-modal feature in most of the seasons and occasionally bi-modal feature during post-monsoon/winter are the common features at the station as reported by Ningombam et al. (2014a).

4.5. HYSPLIT back trajectory analysis

The physical properties of aerosols are strongly dependent on their source of origin, which are widely distributed and highly variable from one region to the other. The present work was also investigated with the Hybrid Single Particle Lagrangian integrated Trajectory (HYSPLIT) air mass back-trajectory analysis for the inferred aerosol types, discussed above. The HYSPLIT model was developed by Draxler and Rolph, at Air Resources Laboratory, NOAA (Draxler and Hess, 1998). In the present study, the back trajectories were calculated pertaining to the height of 1000 m above ground level and for duration of 120 h (five days) for the days categorized for three different types. Further, the Global monthly fire location product (MCD14ML) from the Moderate Resolution Imaging Spectroradiometer (MODIS), on board on Terra spacecraft, was also analyzed and superimposed on air-mass back-trajectory plots to identify the fire-impacted regions of biomass forest fire, surrounding the study region and also to understand the possible transport of generated aerosols from these source regions to the station. More details of the MODIS fire product and fire detection algorithm are given elsewhere (Justice et al., 2002). We also utilize land surface types (particularly arid and desert regions) gridded data (0.167° × 0.167°) retrieved from Clouds and Earths Radiant Energy System (CERES) instrument, onboard Terra spacecraft of NASA. This information is publically available to download via the website http://www-surf.larc.nasa.gov/surf/pages/data-page.html.

Figs. 8(a,b,c) show the air-mass back trajectories for the inferred types at Hanle. All the figures illustrated the locations of arid/semi-arid regions (yellow color: barren/desert and light grey color: open shrub areas) and fire events (red plus marks). In the case of Types I [Fig. 8(a)] and III [Fig. 8(c)], air masses, reaching over the station, are from a broad continental regions comprising with arid/desert and biomass burning areas. It is to be noticed from the figures that on some occasions air masses are coming from the lower heights (mostly from the fire-impacted regions for Type III). On the other hand, in the case of Type II [Fig. 8(b)], the burning activities are relatively low as compared to the case observed for Types I and III. It is clearly evident from the figures that the air masses during this period are transported mostly from the arid/desert regions and which is clearly reflected in the measured aerosol parameters discussed above.

5. Summary and conclusions

Diurnal variation of aerosol optical characteristics was studied from 234 days data of cloud screened data during October 2007–December 2010 from a high-altitude station, Hanle in the western-Himalayas. In the present study, three different types of diurnal AOD were noticed such as (a) Type I: the highest AOD of the day in the forenoon, which gradually decreases in the afternoon and further in the evening, (b) Type II: AOD starts increasing gradually from forenoon to afternoon, attaining a maximum towards the end of the day, and (c) Type III: AOD is low in both the forenoon and the afternoon but increases gradually around local noon-time. The three different Types I,II, and III are accounted for 66 (28%), 41

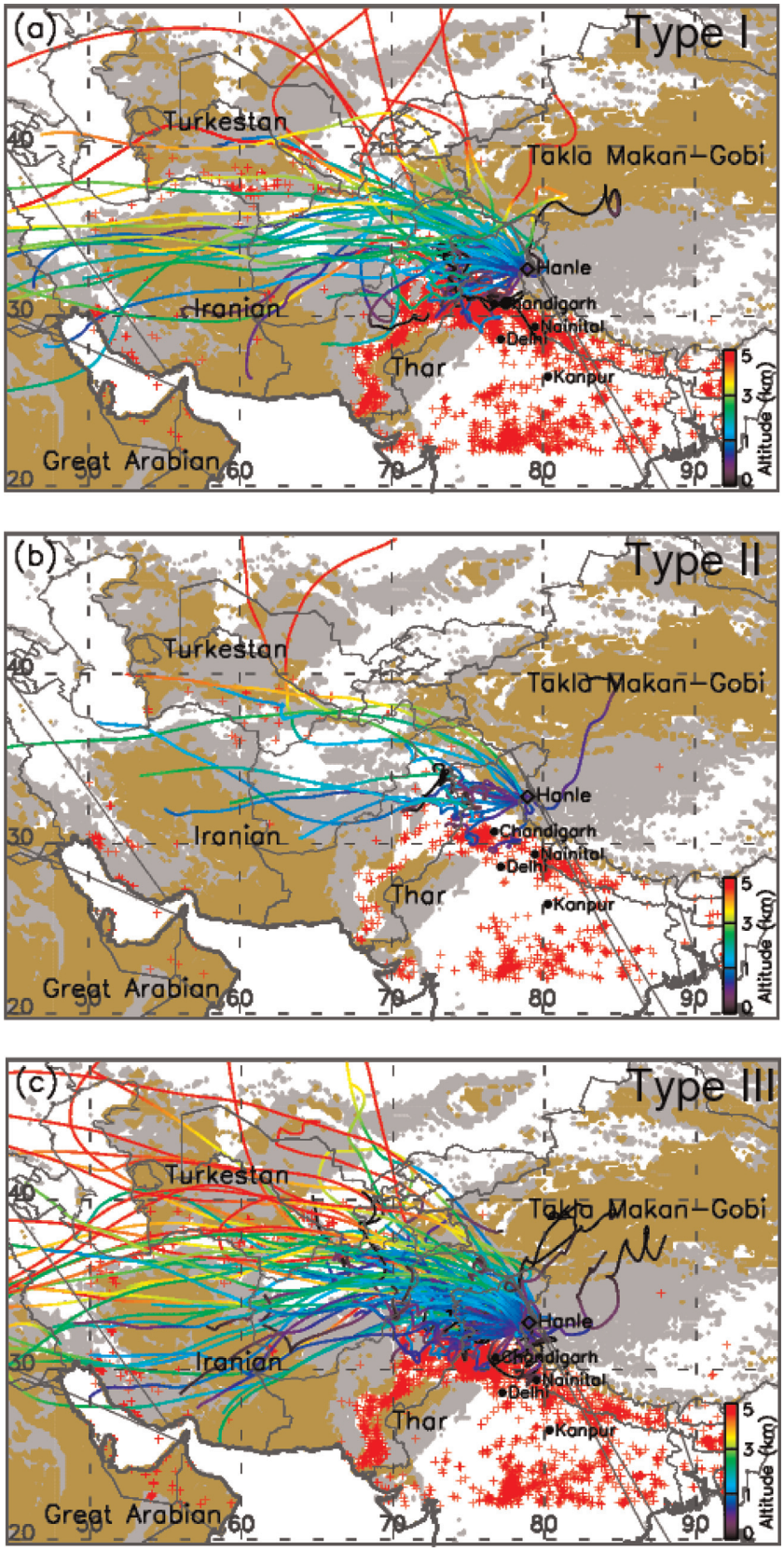

Fig. 8. Back trajectories calculated at 1000 m above the ground level along with the fire counts information from MODIS (on board Terra spacecraft) for the different three types (a,b,c) of diurnal AOD observed at the site. The figures illustrated the locations of arid/semi-arid regions (yellow color:barren/desert and light grey color: open shrub areas) and fire events (red plus marks). (For interpretation of the references to color in this figure caption, the reader is referred to the web version of this paper.)

(18%), and 127 (54%) days, respectively. The mean values of AOD (at 500 nm) for the Types I, II, and III are 0.05, 0.06, and 0.04, respectively. The departure AOD from the daily mean is positive during forenoon and negative during the afternoon for the Type I. However, the departure is negative during forenoon and positive during afternoon for the Type II. The AOD departure is negative at both forenoon and afternoon, but Type III exhibits positive departure near the local noon-time. Non-absorbing features (high single scattering albedo) are seen for the Types I and III, while Type II indicates moderate absorbing features. The Type I and II are occurring more in pre-monsoon season, while Type III occurred more in post-monsoon season.

The mean values of Ångström exponent (α), for the Types I, II, and III are 1.03 ± 0.04, 0.65 ± 0.05, and 0.93 ± 0.03, respectively. Type I appears to be associated with new-particle formation from gaseous precursors, probably carried by the strong westerlies/south-westerlies that prevail during the season in addition to a small contribution from anthropogenic and desert-dust aerosols. The evolution of Type II (though small) can be explained by the dominance of desert-dust aerosols carried by the prevailing westerly/south-westerly winds. Further, Type III may be attributed to aged background aerosols over the region, pertaining to a small contribution from gaseous precursors. The details of such diurnal AOD will be studied further with aerosol radiative forcing over the region.

Acknowledgment

The authors would like to thank the Directors of IIA and IITM for support and encouragement. The authors are particularly thankful to the entire staff of IAO-Hanle, particularly Dorje Angchuk and Stanzin Tundup, for their invaluable assistance during the observations. The Skyradiometer data were analyzed using the Skyrad.pack software, version 4.2 and the authors are thankful to Prof. T. Nakajima for providing the code. The authors acknowledge all the publicly available data set used in the present work such as HYSPLIT back-trajectory calculation, MODIS fire counts, NCEP meteorological fields, and CERES land surface types. Finally, the authors thank the anonymous reviewers for their valuable inputs and suggestions, which helped to improve the quality of the manuscript.

References

Babu, S.S., Chaubey, J.P., Moorthy, K.K., Gogoi, M.M., Kompalli, S.K., Sreekanth, V., Bagare, S.P., Bhatt, B.C., Gaur, V., Prabhu, T.P., Ningombam, S.S., 2011. High altitude (~4520 m amsl) measurements of black carbon aerosols over western Himalayas: seasonal heterogeneity and source apportionment. J. Geophys. Res. 116 (D24), 1984–2012.

Che, H.Z., Wang, Y., Sun, Y., 2011. Aerosol optical properties at Mt. Waliguan Observatory, China. Atmos. Environ. 45 (33), 6004–6009.

Cong, Z., Kang, Shichang, Smirnov, Alexander, Holben, Brent, 2009. Aerosol Optical properties at Nam Co, a remote site in central Tibetan Plateau. Atmos. Res. 92, 42–48.

Draxler, R.R., Hess, G.D., 1998. An overview of the HYSPLIT4 modeling system for trajectories, dispersion, and deposition. Aust. Meteorol. Mag. 47, 295–308.

Gautam, R., Hsu, N.C., Lau, K.M., Tsay, S.C., Kafatos, M., 2009. Enhanced Pre-Monsoon Warming over the Himalayan–Gangetic Region from 1979 to 2007. Geophys. Res. Lett. 36, L07704. http://dx.doi.org/10.1029/2009GL037641.

Gobbi, G.P., Angelini, F., Bonasoni, P., Verza, G.P., Marinoni, A., Barnaba, F., 2010. Sunphotometry of the 2006–2007 aerosol optical/radiative properties at the Himalayan Nepal Climate Observatory-Pyramid (5079 m amsl). Atmos. Chem. Phys. 10, 11209–11221.

Holben, B.N., et al., 2001. An emerging ground-based aerosol climatology: aerosol optical depth from AERONET. J. Geophys. Res. 106 (11), 12067–12097.

Justice, C.O., Gigliob, L., Korontzia, S., Owensa, J., Morisettec, J.T., Roya, D., Descloitresb, J., Alleaumed, S., Petitcoline, F., Kaufman, Y., 2002. The MODIS fire products. Remote Sens. Environ. 83, 244262.

Kaufman, Y.J., Holben, B.N., Tanre, D., Slutsker, I., Smirnov, A., Eck, T.F., 2000. Will aerosol measurements from Terra and Aqua polar orbiting satellites represent the daily aerosol abundance and properties? Geophys. Res. Lett. 23, 3861–3864.

Khatri, P., Takamura, T., 2009. An algorithm to screencloud-affected data for sky radiometer data analysis. J. Meteorol. Soc. Jpn. 87, 189–204.

Kumar, R., Naja, M., Satheesh, S.K., Ojha, N., Joshi, H., Sarangi, T., Pant, P., Dumka, U. C., Hegde, P., Venkataramani, S., 2011. Influences of the springtime northern Indian biomass burning over the central Himalayas. J. Geophys. Res. 116 (D19), D19302. http://dx.doi.org/10.1029/2010jd015509.

Kuniyal, J.C., Thakur, A., Thakur, H.H., Sharma, S., Pant, P., Rawat, P.S., Moorthy, K.K., 2009. Aerosol optical depth at Mohal-Kullu in the northwestern Indian Himalayan high altitude station during ICARB. J. Earth Syst. Sci. 118 (1), 41–48.

Levelt, P.F., et al., 2006. The ozone monitoring instrument. IEEE Trans. Geosci. Remote Sens. 44, 1093–1101.

Liu, Z., et al., 2008. Airborne dust distributions over the Tibetan Plateau and surrounding areas derived from the first year of CALIPSO Lidar observations. Atmos. Chem. Phys. Discuss. 8, 5957–5977.

Moorthy, K.K., Sreekanth, V., Chaubey, J.P., Gogoi, M.M., Babu, S.S., Kompalli, S.K., Bagare, S.P., Bhatt, B.C., Gaur, V.K., Prabhu, T.P., Ningombam, S.S., 2011. Fine and ultrafine particles at a nearfree tropospheric environment over the high-altitude station Hanle in the Trans-Himalaya: new particle formation and size distribution. J. Geophys. Res. 116, D20212. http://dx.doi.org/10.1029/2011JD016343.

McKendry, I.G., Strawbridge, K.B., ONeill, N.T., Macdonald, A.M., Liu, P.S.K., Leaitch, W.R., Anlauf, K.G., Jaegle, L., Fairlie, T.D., Westphal, D.L., 2007. Trans-Pacific transport of Saharan dust to western North America: a case study. J. Geophys. Res. 112, D01103. http://dx.doi.org/10.1029/2006JD007129.

Nakajima, T., Tonna, G., Rao, R., Boi, P., Kaufman, Y., Holben, B.N., 1996. Use of sky brightness measurements from ground for remote sensing of particulate polydispersions. Appl. Opt. 35, 2672–2786.

Ningombam, S.S., 2011. Variability of sunspot cycle, QBO and total ozone over high altitude western Himalayan regions. J. Atmos. Solar Terr. Phys. 73, 2305–2313.

Ningombam, S.S., Bagare, S.P., Sinha, N., Singh, R.B., Srivastava, A.K., Larson, E., Kanawade, V.P., 2014a. Characterization of aerosol optical properties over the high altitude station Hanle, in the trans-Himalayan region. Atmos. Res. 138, 308–323.

Ningombam, S.S., Bagare, S.P., Singh, R.B., Campanelli, M., Khatri, P., Dorjey, N., 2014b. Calibration of a Sky radiometer (Prede) using observations obtained from Hanle and Merak high-altitude stations in Ladakh. Atmos. Res. 143, 118–128.

Neitola, K., Asmi, E., Komppula, M., Hyvrinen, A.-P., Raatikainen, T., Panwar, T.S., Sharma, V.P., Lihavainen, H., 2011. New particle formation infrequently observed in Himalayan foothills why? Atmos. Chem. Phys. 11, 8447–8458.

Pinker, R.T., Idemundia, G., Aro, T.O., 1994. Characteristics aerosol optical depths during the Harmattan season on sub-Sahara Africa. Geophys. Res. Lett. 21, 685–688.

Powell, K.A., Chris, A., Hostetler, Mark A., Vaughan, Kam-Pui Lee, Trepte, Charles R., Rogers, Raymond R., Winker, David M., Liu, Zhaoyan, Kuehn, Ralph E., Hunt, William H., Young, Stuart A., 2009. CALIPSO lidar calibration algorithms. Part I: Nighttime 532-nm parallel channel and 532-nm perpendicular channel. J. Atmos. Ocean. Technol. 26 (10), 2015–2033.

Ram, K., Sarin, M.M., Hegde, P., 2010. Long-term record of aerosol optical properties and chemical composition from a high-altitude site (Manora Peak) in Central Himalaya. Atmos. Chem. Phys. 10 (23), 11791–11803.

Sagar, R., Kumar, B., Dumka, U.C., Moorthy, K.K., Pant, P., 2004. Characteristics of aerosol spectral optical depth over Manora peak: a high-altitude station in the central Himalayas. J. Geophy. Res. 109, D06207. http://dx.doi.org/10.1029/2003JD003954.

Seinfeld, J.H., et al., 2004. ACE-ASIA regional climatic and atmospheric chemical effects of Asian dust and pollution. Bull. Am. Meteorol. Soc. 85, 367–380. http://dx.doi.org/10.1175/BAMS-85-3-367.

Six, D., Fily, M., Blarel, L., Goloub, P., 2005. First aerosol optical thickness measurements at Dome C (East Antarctica) summer season 2003–2004. Atmos. Environ. 39, 5041–5050.

Smirnov, A., Villevalde, Y., O'Neill, N.T., Royer, A., Tarussov, A., 1995. Aerosol optical depth over the oceans: analysis in terms of synoptic air mass types. J. Geophy. Res. 100, 16639–16650.

Smirnov, A., Holben, B.N., Eck, T.F., Slusker, I., Chatenet, B., Pinker, R.T., 2002. Diurnal variability of aerosol optical depth observed at AERONET Sites. Geophys. Res. Lett. 29 (23), 2115. http://dx.doi.org/10.1029/2002GL016305.

Srivastava, A.K., Pant, P., Hegde, P., Singh, S., Dumka, U.C., Naja, M., Singh, N., Bhavanikumar, Y., 2011. The influence of a south Asian dust storm on aerosol radiative forcing at a high-altitude station in central Himalayas. Int. J. Remote Sens. 32 (22), 7827–7845.

Srivastava, A.K., Ram, K., Pant, P., Hegde, P., Joshi, H., 2012. Black carbon aerosols over Manora Peak in the Indian Himalayan foothills: implications for climate forcing. Environ. Res. Lett. 7, 014002. http://dx.doi.org/10.1088/1748-9326/7/1/014002.

Srivastava, A.K., Singh, S., Pant, P., Dumka, U.C., 2012b. Characteristics of black carbon over Delhi and Manora Peak—a comparative study. Atmos. Sci. Lett. 13, 223–230.

Toledano, C., Wiegner, M., Garhammer, M., et al., 2009. Spectral aerosol optical depth characterization of desert dust during SAMUM 2006. Tellus 61 (1), 216–228.

Verma, N., Bagare, S.P., Ningombam, S.S., Singh, R.B., 2010. Aerosol optical properties retrieved using skyradiometer at hanle in western Himalayas. J. Atmos. Solar Terr. Phys. 72, 115–124.